Surface states on NiO (100) and the origin of the contrast reversal in atomically resolved scanning tunneling microscope images

S. L. Dudarev
Department of Materials, University of Oxford, Parks Road, Oxford OX1 3PH, United Kingdom

A. I. Liechtenstein
Forschungszentrum Julich, D-52425 Julich, Germany

M. R. Castell, G. A. D. Briggs, and A. P. Sutton
Department of Materials, University of Oxford, Parks Road, Oxford OX1 3PH, United Kingdom

(Received 20 February 1997)

The local spin-density approximation+U method has been applied to identify the origin of surface electronic states on the (100) surface of nickel monoxide. The results of *ab initio* calculations show a substantial reduction of the forbidden gap at the surface and point to the presence of two types of electronic states associated with the termination of the crystal lattice. The energy of one of the surface states corresponds to the top of the valence band and the wave function of this state is predominantly localized on the oxygen surface sites. The other state is situated at the bottom of the conduction band and its wave function is localized on the nickel sites. The presence of these surface states explains the origin of the contrast reversal of scanning tunneling microscope images of the (100) NiO surface observed experimentally by altering the sign of the bias applied to the sample. [S0163-1829(97)00632-2]

I. INTRODUCTION

The surfaces of transition-metal oxides (TMO's) play an important role in a wide range of phenomena and there is growing interest in various technological applications of oxides in chemistry and materials science.[1] Since the electronic structure of a surface can differ significantly from the electronic structure of the bulk material,[2] it appears that transitions between *surface* electronic states, rather than between *bulk* electronic states, are responsible for many interesting properties of TMO's.[3]

The electronic structure of a large number of TMO's is dominated by the presence of strong on-site Coulomb repulsion (strong correlations) between d electrons localized on transition metal ions. Since d orbitals of metal ions, together with p orbitals of oxygen ions, constitute the electronic states of interest near the Fermi energy, the problem of an adequate description of correlation effects in an *ab initio* computational scheme turns out to be of fundamental importance for predicting the bulk and surface properties of TMO's from first principles. For many years the question of the applicability of the local spin-density approximation (LSDA) to the description of the electronic structure of TMO's remained a subject of intense debate.[4–7] More recently, several alternative *ab initio* approaches to the description of the electronic structure of bulk TMO's have been developed to explain, sometimes qualitatively and in some cases quantitatively, experimental results that have accumulated over the past decade, mainly from x-ray photoelectron spectroscopy.[8–10] These *ab initio* methods include the GW treatment of nickel monoxide developed by Aryasetiawan and Gunnarsson,[11] the three-particle correction to the LSDA proposed by Manghi *et al.*,[12] the Hartree-Fock study by Towler *et al.*[13] and the LSDA+U method developed by Anisimov *et al.*[14] and reformulated into a rotationally invariant form by Liechtenstein *et al.*[15] There is a growing consensus that nickel monoxide belongs to the class of charge transfer insulators, and that its bulk electronic structure is characterized by the predominantly Ni d-like conduction band, and that the top of the valence band has predominantly O p-like character.[16,17] The insulating behavior of NiO is associated with a large Hubbard splitting of filled and empty d states separated by $U \approx 8$ eV, which is twice the width of the band gap $E_g \approx 4$ eV.[17]

The amount of reliable information about the electronic structure of *surfaces* of TMO's is relatively limited. Partly this results from the fact that many of the TMO's are room temperature insulators and this makes them far more difficult to study than conventional metals or semiconductors. X-ray photoelectron spectroscopy (XPS), which has provided the largest amount of reliable experimental information about bulk electronic states in TMO's,[9,10] appears to be less sensitive to the electronic structure of surface atomic layers. More surface sensitive electron energy loss spectroscopy (EELS) measurements[18–20] carry information about the spectrum of excitations conserving the number of electrons in the system. As a result, EELS results are often harder to interpret than XPS observations since the latter provide information in a somewhat simpler form of electron addition or electron removal spectra.[16]

Very recently there has emerged a new technique for studying the electronic and atomic structures of TMO surfaces, namely, elevated temperature scanning tunneling microscope (STM) imaging.[21–23] It has been demonstrated that elevated temperature STM can be successfully employed to obtain atomically resolved images of flat and defective surfaces of various materials that are insulators at room temperature. Since the signal that forms an STM image is pro-

duced by adding or removing electrons from the surface, the interpretation of the resulting image appears to be similar to the interpretation of an XPS spectrum. However, this analogy should not be carried too far since there are two important factors which distinguish the two techniques. First, the spatial resolution (in the plane parallel to the surface) that can be achieved using STM is many orders of magnitude higher than the resolution accessible to XPS. For example, a scanning tunneling microscope has made it possible to observe individual point defects on a NiO surface.[23] Second, to interpret a STM image one needs to know the *surface* electronic structure, e.g., the density of single-particle surface states. This poses a problem that is more demanding computationally than a calculation of the single-particle density of states (DOS) for a unit cell in the crystal bulk.

In the past, several calculations have been performed aimed at understanding the electronic structure of nickel monoxide surfaces. Lee and Wong[24] extended the linear combination of atomic orbitals treatment of NiO developed by Mattheiss[25] and used his parametrization of the tight-binding matrix elements to study the electronic structure of the (100) surface. However, the authors of Ref. 24 did not recognize the fact that, according to their treatment, nickel monoxide was predicted to be metallic, and they erroneously identified the band gap as a gap between filled oxygen and *filled* nickel states (cf. a review by Adler.[4])

A configuration-interaction (CI) approach to the calculation of energies of the ground and excited states of Ni ions located in the first atomic plane of the NiO (100) surface has been developed by Freitag *et al.*[19] The calculation was carried out for a cluster of one Ni and five O ions embedded in a semi-infinite lattice of pointlike ions representing the remaining nickel and oxygen sites. Freitag *et al.* showed that the energies of the excited states calculated using the CI approach corresponding to the dipole-forbidden *d*-*d* transitions were in good agreement with the results of high-resolution EELS measurements. Extensive experimental EELS studies carried out by Gorschlüter and Merz[20] have confirmed the above findings. For the purpose of comparison with the results of the LSDA+U calculation discussed below we note that the CI analysis[19,20] was focused on intracluster excitations, the energies of which did not exceed the width of the band gap. By contrast in this work we treat a much broader range of energies within an effective one-electron picture.

More recently it has been shown that the effects associated with covalent coupling between the central ion of a cluster and its nearest and even next nearest neighbors may play an important role, and may give rise to a number of readily observed phenomena.[26,27] The presence of strong covalent coupling between next nearest neighbors in the Ni sublattice has also been observed in STM images in the form of $c(2\times2)$ patterning around defect sites and step edges.[23] These observations suggest that it is desirable to carry out an *ab initio* study of the NiO surface using a method which does not rely on a cluster-type geometry.

In this paper we study the electronic structure of the NiO (100) surface using the so-called LSDA+U approach. This approach was proposed by Anisimov *et al.*[14] as a relatively simple way of bridging the gap between the conventional methods based on LSDA and the Hubbard model. The LSDA+U method can therefore be viewed as an approach which provides an alternative to the cluster-based treatment of the electronic structure of TMO's. In LSDA+U the solid is treated as a periodic continuum and correlation effects are included using a special form of the effective one-electron potential which acts differently on the occupied and unoccupied electronic orbitals. One of the main achievements of the LSDA+U method was an order of magnitude improvement over the previously known LSDA results in the calculated width of band gaps for a number of compounds including TMO's (Ref. 14) and actinide oxides.[28] Subsequent analysis[17] has shown that the DOS calculated using the LSDA+U approach agrees with experimental XPS spectra and also with the results obtained using the Anderson impurity model.[16] Below we apply the LSDA+U method in order to understand the electronic structure of the (100) surface of nickel monoxide, and to explain the origin of the contrast reversal of images observed when the applied sample bias in an elevated temperature scanning tunneling microscope is reversed.[23] Our analysis also allows us to explain why it is much harder to obtain atomically resolved STM images at negative sample bias compared with positive bias.

II. THE LSDA+U METHOD

To explain the idea of the rotationally invariant LSDA+U method[15] let us consider the difference between electrons interacting as parts of an individual ion or as constituents of an ion embedded in a solid or a liquid. The energy of electron-electron interaction is given by the expectation value of the relevant part of the Hamiltonian[29]

$$\hat{H}_{\rm int}=\frac{1}{2}\sum_{\sigma,\sigma'}\int d\mathbf{r}d\mathbf{r}'\hat{\Psi}^{\dagger}_{\sigma}(\mathbf{r})\hat{\Psi}^{\dagger}_{\sigma'}(\mathbf{r}')V_c(\mathbf{r},\mathbf{r}')\times\hat{\Psi}_{\sigma'}(\mathbf{r}')\hat{\Psi}_{\sigma}(\mathbf{r}),\tag{1}$$

where $V_c(\mathbf{r},\mathbf{r}')$ is the potential of the screened Coulomb interaction, averaged over the (variational) ground state of the system $|\Phi\rangle$. In the case of an individual ion the Ψ operators entering Eq. (1) may be expressed in terms of a set of atomic orbitals $\{\phi_j(\mathbf{r})\}$ representing the eigenfunctions of the system:

$$\hat{\Psi}_{\sigma}(\mathbf{r})=\sum_j \phi_j(\mathbf{r})\hat{a}_{j\sigma},\tag{2}$$

where σ denotes the projection of spin. This leads to the standard Hartree-Fock expression for the energy of electron-electron interaction,

$$\langle\Phi|\hat{H}_{\rm int}|\Phi\rangle=\frac{1}{2}\sum_{j,k}\sum_{\sigma,\sigma'}(\langle jk|\hat{H}_{\rm int}|jk\rangle n_{j\sigma}n_{k\sigma'}-\delta_{\sigma\sigma'}\langle jk|\hat{H}_{\rm int}|kj\rangle n_{j\sigma}n_{k\sigma}),\tag{3}$$

where $n_{j\sigma}=\langle\Phi|\hat{a}^{\dagger}_{j\sigma}\hat{a}_{j\sigma}|\Phi\rangle$ are the occupation numbers of the relevant orbitals and

$$\langle jk|\hat{H}_{\rm int}|lm\rangle=\int d\mathbf{r}d\mathbf{r}'\,\phi^{*}_j(\mathbf{r})\phi^{*}_k(\mathbf{r}')V_c(\mathbf{r},\mathbf{r}')\phi_l(\mathbf{r})\phi_m(\mathbf{r}').\tag{4}$$

Since the states $|\phi_j\rangle$ are the eigenstates of an individual ion, the occupation numbers $n_{j\sigma}$ equal either 1 or 0.

If an ion is embedded in a solid and the amplitude of electron hopping between ions is substantial, the evaluation of the expectation value $\langle\Phi|\hat{H}_{\rm int}|\Phi\rangle$ requires that the Ψ operators are expressed in terms of creation and annihilation operators of quasiparticles

$$\hat{\Psi}_\sigma(\mathbf{r})=\sum_\alpha \chi_\alpha(\mathbf{r})\hat{a}_{\alpha\sigma}, \tag{5}$$

the wave functions of which are now linear combinations of atomic orbitals $\chi_\alpha(\mathbf{r})=\Sigma_j A_{j\alpha}\phi_j(\mathbf{r})$. The expectation value of the energy of interaction between electrons occupying atomic orbitals of an ion is now given by

$$\langle\Phi|\hat{H}_{\rm int}|\Phi\rangle=\frac{1}{2}\sum_{j,k,l,m}\sum_{\sigma,\sigma'}(\langle jk|\hat{H}_{\rm int}|lm\rangle\rho^\sigma_{lj}\rho^{\sigma'}_{mk} - \delta_{\sigma\sigma'}\langle jk|\hat{H}_{\rm int}|lm\rangle\rho^\sigma_{mj}\rho^\sigma_{lk}), \tag{6}$$

where $\rho^\sigma_{lj}=\Sigma_\alpha A_{l\alpha}n_{\alpha\sigma}A^*_{j\alpha}$ is the density matrix[30] and $n_{\alpha\sigma}=0,1$ are the quasiparticle occupation numbers. The appearance of the density matrix in Eq. (6) is not surprising since an ion embedded in a solid represents an open system interacting with the environment and therefore its quantum state cannot generally be described by a wave function[30] (unless this state is a pure state) nor can it be characterized by a set of occupation numbers $\{n_{j\sigma}\}$ of a set of fixed basis functions. We also note that since Eq. (6) has the form of a trace of a product of matrices, it is invariant with respect to any unitary (for example, rotational) transformation of the basis functions $\{\phi_j(\mathbf{r})\}$.

Now, following the methodology of the LSDA+U approach, we note that for the majority of orbitals (in the case of a transition-metal ion we mean all orbitals except those belonging to the partly filled d shell) the expectation value of the Hamiltonian (1) may be cast in the form of a functional of the density of electrons $n_\sigma(\mathbf{r})$. However, for a localized orbital (e.g., for the d orbital of a transition metal ion), the appropriate form of this functional remains unknown. It is known that the major source of error of conventional LSDA calculations in the present context is associated with an inadequate description of the Coulomb interaction between electrons occupying a localized orbital. We therefore focus on the *difference* between the expectation value of $\hat{H}_{\rm int}$ calculated using a localized basis set (6), and the corresponding quantity $\langle\Phi|\hat{H}_{\rm int}|\Phi\rangle_{\rm LSDA}$ evaluated assuming that it is a functional of $n_\sigma(\mathbf{r})$ (or, as in the case of the d orbital, is a function of the total number of electrons with a given projection of spin in this shell). Since for any choice of the basis functions there always exists a unitary transformation diagonalizing ρ^σ_{lj} for a given orbital, we arrive at

$$\langle\Phi|\hat{H}_{\rm int}|\Phi\rangle_{\rm LSDA}=\frac{U}{2}(N_\uparrow+N_\downarrow)(N_\uparrow+N_\downarrow-1) - \frac{J}{2}[N_\uparrow(N_\uparrow-1)+N_\downarrow(N_\downarrow-1)], \tag{7}$$

where U and J are the screened Coulomb and exchange parameters[31] and $N_\uparrow$ and $N_\downarrow$ are the total numbers of electrons with spin up (down) occupying the d orbital of one of the transition metal ions. Subtracting Eq. (7) from Eq. (6) and differentiating the result with respect to ρ^σ_{lj}, we obtain the required invariant form of the LSDA+U correction ΔV^σ_{jl} to the effective one-electron potential V^σ_{jl}, namely,

$$\begin{aligned}\Delta V^\sigma_{jl}&\equiv\frac{\delta}{\delta\rho^\sigma_{lj}}[\langle\Phi|\hat{H}_{\rm int}|\Phi\rangle-\langle\Phi|\hat{H}_{\rm int}|\Phi\rangle_{\rm LSDA}]\\ &=\sum_{m,k}[\langle jk|\hat{H}_{\rm int}|lm\rangle\rho^{-\sigma}_{mk}+(\langle jk|\hat{H}_{\rm int}|lm\rangle\\ &\quad-\langle jk|\hat{H}_{\rm int}|ml\rangle)\rho^\sigma_{mk}]-U\delta_{jl}\left[\left(\sum_{\sigma',k}\rho^{\sigma'}_{kk}\right)-\frac{1}{2}\right]\\ &\quad+J\delta_{jl}\left[\left(\sum_k\rho^\sigma_{kk}\right)-\frac{1}{2}\right].\end{aligned} \tag{8}$$

This simple formula (8) can be used as a correction to the exchange-correlation potential of density-functional theory to describe correlations between valence electrons occupying localized orbitals. In what follows we consider an application of the above formalism to the case of nickel monoxide where this correction has been added to the effective potential acting on electrons occupying d orbitals of Ni ions.

III. ELECTRONIC STATES ON THE (100) SURFACE OF NICKEL MONOXIDE

The results described below have been obtained using a modified version of the LSDA+U method implemented with the full-potential code written by Savrasov and Savrasov[32] and Liechtenstein.[15] Since we are interested in understanding the origin of the changes in the electronic structure associated with the termination of the crystal lattice, it is useful to consider first the electronic structure of *bulk* nickel monoxide. Figure 1 shows a plot of the density of d states of nickel ions and the density of p states of oxygen ions. The calculation was performed assuming that the lattice constant of NiO is $a_0=4.194$ Å ($=7.927$ a.u.) and that the radii of the muffin-tin (MT) spheres are equal to $R_{\rm Ni}=2.076$ a.u. and $R_{\rm O}=1.887$ a.u. In choosing the values of U and J we followed Ref. 14 and assumed $U=F^0=8.0$ eV and $J=(F^2+F^4)/14=0.95$ eV. The resulting insulating antiferromagnetic ground state of NiO is characterized by a magnetic moment of $\mu=1.74\mu_B$ per Ni site and by a band gap, E_g, of 3.50 eV. In agreement with the results obtained previously using a different version of the LSDA+U method,[17] the electronic structure of NiO in the vicinity of the Fermi energy is characterized by a broad forbidden gap above the valence band which consists of filled oxygen p states and a smaller admixture of nickel t_{2g} and e_g d states. Therefore, the top of the valence band has predominantly oxygen p character. The conduction band is formed by weakly hybridized empty e_g states of Ni ions with a small (although identifiable) admixture of oxygen p states. This picture contrasts with the result of an LSDA calculation predicting only a very narrow ($\sim$0.2 eV) band gap separating filled *nickel* d and empty nickel d states. Since this value of the band gap does not agree with the results of our experimental STM work described in Ref. 23, we conclude that the density of one-

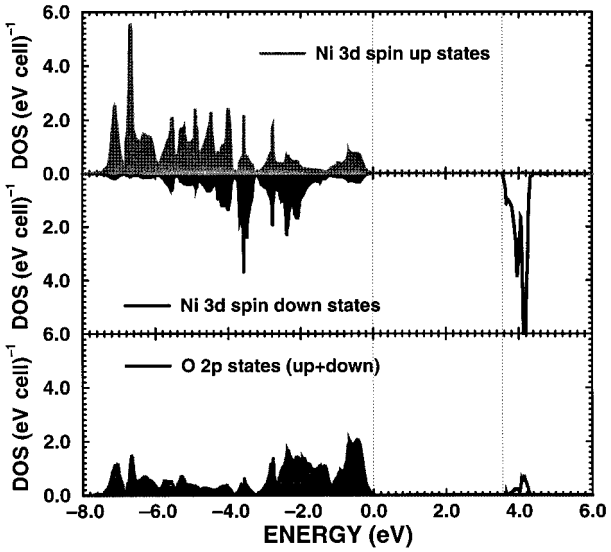

FIG. 1. Projected DOS of bulk nickel monoxide calculated in the LSDA+U approximation with a lattice constant of $a_0=7.927$ a.u. and assuming $F^0=8.0$ eV, $F^2=8.21$ eV, and $F^4=5.15$ eV. The ground state of NiO is antiferromagnetic and insulating with a band gap of approximately 3.5 eV.

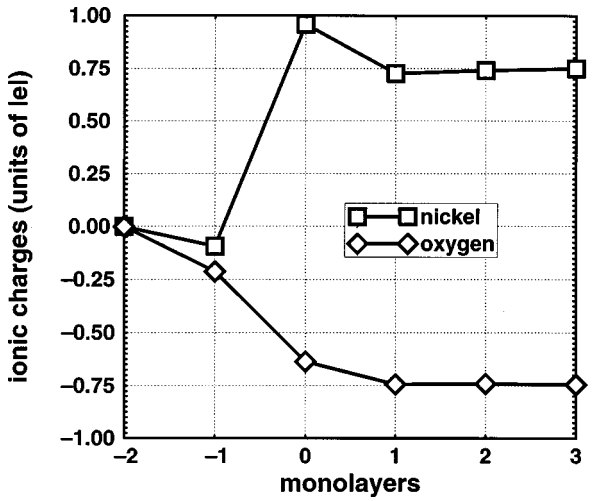

FIG. 2. Distribution of charges of nickel and oxygen ions near the (100) surface of nickel monoxide calculated using the LSDA $+U$ approach. The calculation was performed assuming a bulk terminated crystal structure and bulk values of the parameters U and J characterizing the Coulomb on-site interaction between nickel d electrons. Charges corresponding to the vacuum region have been evaluated for empty spheres situated above nickel and oxygen surface lattice sites.

particle electronic states calculated using LSDA cannot be used to explain the contrast of STM images.

In order to analyze the electronic structure of the (100) surface, we have carried out a series of calculations assuming that nickel and oxygen ions occupy lattice sites belonging to a periodic system of slabs separated by layers of empty spheres. We have found that in order to reach a convergent result we had to use a geometry in which every seven layers of nickel monoxide were separated by six layers of empty spheres. To describe Coulomb repulsion between electrons in the 3d shell of Ni atoms, in our slab calculations we used the same values of $U=8.0$ eV and $J=0.95$ eV that we employed when we analyzed the band structure of bulk NiO. It is likely that weakening of screening of electron-electron interactions at the crystal-vacuum interface may give rise to a larger value of U for nickel ions situated on the surface. However, given that the predominant contribution to screening comes from electrons belonging to the same ion,[31] the expected modification of the value of U associated with the presence of the surface is likely to be relatively small and in the context of the present study may be disregarded.

To assess the behavior of the tails of wave functions propagating into the vacuum region, we analyzed the densities of 1s states centered on empty lattice sites. In our calculations we assumed that the atomic structure of the NiO (100) surface is an ideal termination of the bulk crystal structure with no relaxation. This assumption is based on experimental low-energy electron diffraction data showing no detectable rumpling and an inward surface relaxation not exceeding $\sim 2\%$.[33,34] The ground state of NiO found in our slab calculation was antiferromagnetic with magnetic moments localized on Ni sites. The magnitude of the magnetic moments was found to be less than 2% different from the corresponding bulk value of $1.74\mu_B$, i.e., $1.72\pm 1\mu_B$.

In Fig. 2 the distribution of ionic charges near the (100) surface of NiO is shown as a function of the atomic layer number M. Positive $M=0,1,2,3$ corresponds to layers filled with oxygen and nickel ions while negative $M=-1,-2$ corresponds to vacuum layers filled with empty spheres. The fact that the bulk asymptotic values of ionic charges $Z_{\mathrm{Ni}}\approx +0.75$ and $Z_{\mathrm{O}}\approx -0.75$ do not coincide with the expected standard ''ionic'' values $Z_{\mathrm{Ni}}=+2$ and $Z_{\mathrm{O}}=-2$ is associated with the known arbitrariness of the definition of ionic charges. Indeed, due to the delocalization of electronic orbitals the magnitude of ionic charges depends largely on the choice of the MT sphere radii. Nevertheless, despite the presence of this arbitrariness, it is possible to observe trends associated with the redistribution of electron density near the surface. Figure 2 shows that the surface Ni ions are substantially more positively charged than Ni ions situated in the crystal bulk. The surface oxygen ions turn out to be less negatively charged than oxygen ions in the crystal bulk. Global charge neutrality conservation is maintained through the differing amounts of charge spilling into the vacuum region from oxygen and nickel ions.

To understand the origin of the changes in the electronic structure of nickel monoxide associated with the termination of the crystal lattice, in Figs. 3 and 4 we have plotted the DOS of nickel 3d states and oxygen 2p states for bulk and several surface atomic layers parallel to the (100) plane. The plots at the top of both figures show the density of 1s states localized in empty spheres positioned in the vacuum region above nickel and oxygen surface sites. The DOS shown in Figs. 3 and 4 were evaluated using 45 k points. Figures 3 and 4 show a reduction of the forbidden gap separating the filled (hole) and empty (electron) states at the surface (for the case shown in Figs. 3 and 4, $E_g\approx 3.31$ eV). The primary reason for this reduction is the modification of the Madelung potential for ions situated at the surface. The change in the Madelung energy at the surface, which is associated with the termination of the crystal lattice, increases on-site energies of electronic states at oxygen sites and reduces them at nickel sites. The existence of this effect was pointed out by Pothui-

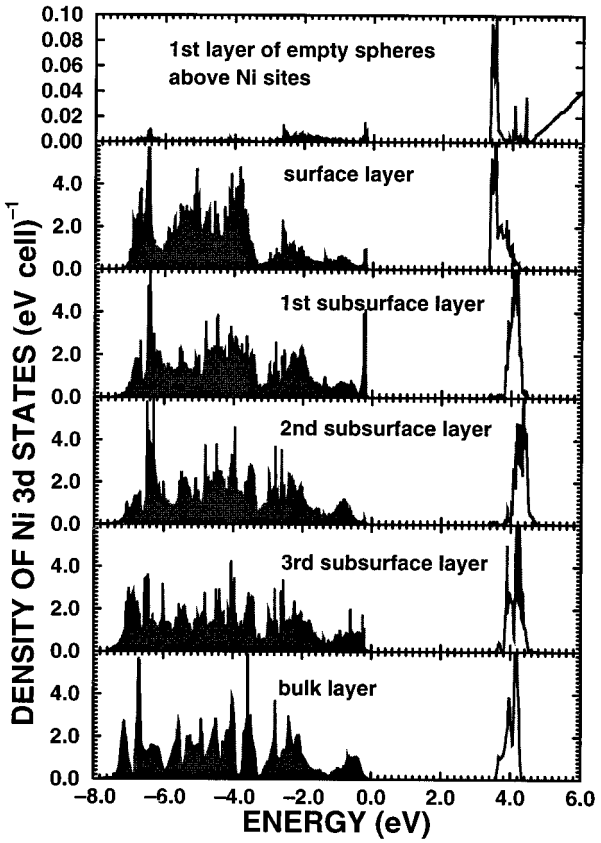

FIG. 3. Projected DOS of nickel 3*d*-states evaluated for nickel ions belonging to the first four surface layers of nickel monoxide. The top panel shows the density of 1*s* states corresponding to empty spheres in the vacuum region above the nickel sites. The chemical potential is in the middle of the band gap.

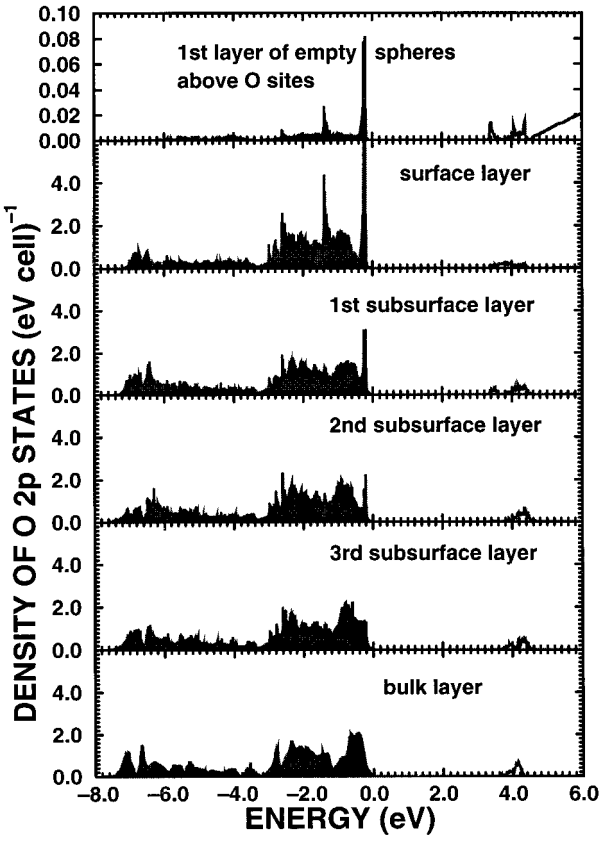

FIG. 4. Projected DOS of oxygen 2*p* states evaluated for oxygen ions belonging to the first four surface layers of nickel monoxide. The top panel shows the density of 1*s* states corresponding to empty spheres in the vacuum region above the oxygen sites.

zen and Sawatzky[35] but the magnitude of the effect, according to our calculations, appears to be somewhat smaller than that estimated on the basis of an ionic model in Ref. 35.

The DOS spectra shown in Figs. 3 and 4 exhibit two sharp peaks at opposite edges of the forbidden gap. The importance of these two peaks becomes apparent from a comparison between DOS calculated for the surface layer and for the first layer of empty spheres. Indeed, these peaks give rise to the highest peaks in the DOS of the first ''vacuum'' layer. To understand the origin of these surface states consider the crystal-field splitting of oxygen *p* and nickel *d* states in the electrostatic field of C_{4v} symmetry created by the five nearest neighbors of a given ion at the surface (note that in the bulk there is no splitting of either oxygen *p* or nickel *d* e_g states). A simple perturbation calculation[36] for oxygen *p* states results in

$$\epsilon_x=\epsilon_y=\frac{5Z_{\mathrm{Ni}}e^2}{a_0}-\frac{1}{5}\frac{Z_{\mathrm{Ni}}e^2}{a_0}\frac{\langle r^2\rangle_p}{a_0^2},$$

$$\epsilon_z=\frac{5Z_{\mathrm{Ni}}e^2}{a_0}+\frac{2}{5}\frac{Z_{\mathrm{Ni}}e^2}{a_0}\frac{\langle r^2\rangle_p}{a_0^2}, \tag{9}$$

where $\langle r^2\rangle_p=\int dr r^4|R_{l=1}(r)|^2$ and $Z_{\mathrm{Ni}}>0$ is the effective charge of a nickel ion. Hence the top of the valence band at the (100) surface is formed by oxygen *p* states of p_z symmetry.

A similar calculation for the two nickel *d* e_g states forming the conduction band gives rise to

$$\epsilon_{3z^2-r^2}=\frac{5Z_{\mathrm{O}}e^2}{a_0}+\frac{2}{7}\frac{Z_{\mathrm{O}}e^2}{a_0}\frac{\langle r^2\rangle_d}{a_0^2},$$

$$\epsilon_{x^2-y^2}=\frac{5Z_{\mathrm{O}}e^2}{a_0}-\frac{2}{7}\frac{Z_{\mathrm{O}}e^2}{a_0}\frac{\langle r^2\rangle_d}{a_0^2}, \tag{10}$$

where $\langle r^2\rangle_d=\int dr r^4|R_{l=2}(r)|^2$ and $Z_{\mathrm{O}}<0$ is the effective ionic charge of an oxygen ion. Equation (10) shows that the bottom edge of the conduction band is formed by nickel *d* states of $d_{3z^2-r^2}$ symmetry. Figures 3 and 4 therefore show that oxygen p_z states and Ni $d_{3z^2-r^2}$ states are responsible for the behavior of wave functions in the vacuum region above the (100) surface. These figures also show that the surface states are not confined to the first surface layer, but that they penetrate to the subsurface and even the second subsurface layers. This penetration of surface states into subsurface layers is mediated by strong covalent coupling between oxygen p_z states and nickel $d_{3z^2-r^2}$ states, which gives rise to an effective second nearest neighbor Ni-Ni coupling. Enhanced second nearest neighbor coupling, due to strong nearest neighbor Ni-O covalent bonding, is consistent with experimental results[27,23] for NiO showing strong second nearest neighbor coupling in the plane of the (100) surface.

IV. THE ORIGIN OF THE CONTRAST REVERSAL OF STM IMAGES

We now address the interpretation of two experimental STM observations of the NiO (100) surface. The first concerns the contrast reversal that has been observed[23] at positive and negative bias. The second observation concerns the lower contrast that is found at negative rather than at positive sample bias. We will show how both observations may be interpreted theoretically.

Recent atomically resolved STM observations of the NiO (100) surface[23] have shown that at positive sample bias (corresponding to imaging *via* empty states in the NiO) the Ni sublattice is imaged. At negative sample bias (corresponding to imaging *via* filled states in the NiO) the oxygen sublattice is seen. Thus, there is a reversal in the contrast seen under positive and negative biases.

In the previous section we showed that the electronic structure of the (100) surface is characterized by the presence of two types of surface states. At the top of the valence band there are filled surface states consisting primarily of oxygen p_z orbitals. Empty surface states beneath the bottom of the conduction band are constituted primarily from nickel $d_{3z^2-r^2}$ orbitals. It is well established that surface states may make a substantial, and sometimes dominant, contribution to the tunneling current.[37] We will show that the reason for the contrast reversal is that tunneling into the sample at positive bias occurs through the unoccupied surface states centered primarily on *nickel* sites, whereas at negative sample bias tunneling out of the sample occurs from the occupied surface state centered primarily on *oxygen* sites.

In the Bardeen approximation the tunneling current is proportional to the square of the transition matrix element t_{TS} between electronic states Ψ_T and Ψ_S belonging to the tip and the sample. The magnitude of this matrix element is given by

$$t_{\mathrm{TS}}=\frac{\hbar^2}{2m}\int_A d\mathbf{A}\Big[\Psi_T(x,y,z_A(x,y))\frac{\partial}{\partial\mathbf{r}}\Psi_S^*(x,y,z_A(x,y)) - \Psi_S^*(x,y,z_A(x,y))\frac{\partial}{\partial\mathbf{r}}\Psi_T(x,y,z_A(x,y))\Big], \tag{11}$$

where the integration is performed over an arbitrary surface A separating the entire space into two parts, one including the tip and the other including the sample in such a way that the effective one-electron potential vanishes everywhere at this surface. The tunneling current can be evaluated by applying the standard expression from perturbation theory

$$I=\frac{2\pi}{\hbar}\sum_{S,T}(n_T-n_S)|t_{\mathrm{TS}}|^2\delta(E_T-E_S), \tag{12}$$

where n_T and n_S are the occupation numbers of quasiparticle states of the tip and sample, respectively. For a finite absolute temperature Θ these occupation numbers are

$$n_T=[\exp(E_T/k_B\Theta)+1]^{-1},$$
$$n_S=[\exp(E_S/k_B\Theta)+1]^{-1}, \tag{13}$$

where the definition of E_T includes the shift associated with the applied bias. From Eqs. (11) and (12) it follows that the contrast of an STM image may be understood qualitatively in terms of the distribution of charge density in the vacuum region above the surface (see, e.g., a recent analysis of STM images of TiO_2 by Diebold *et al.*[38]) In our case, therefore, we identify the sublattices seen at positive and negative bias, by comparing the charge densities at the relevant energies in the empty spheres above the surface.

We have adopted a simple procedure that enables us to represent the results in the form of a black and white pattern that may be compared with STM images. The DOS of Figs. 3 and 4 show that the dispersion of the two bands of surface states, seen at the two edges of the forbidden gap, is small. These states can therefore be viewed as a sequence of almost nonoverlapping filled p_z and empty $d_{3z^2-r^2}$ orbitals sticking out of the surface from oxygen and nickel surface lattice sites, respectively. This is seen clearly in the spectra of $1s$ states associated with the first layer of empty spheres. If we consider a $1s$ orbital of the form

$$\Psi_s(\mathbf{r})=\frac{\mathcal{A}(E)}{|\mathbf{r}-\mathbf{r}_0|}\exp\left(-\sqrt{\frac{2m|E|}{\hbar^2}}|\mathbf{r}-\mathbf{r}_0|\right), \tag{14}$$

centered at a particular point $\mathbf{r}_0$ in the vacuum region, it follows that the amplitude $\mathcal{A}(E)$ is related to the density $D_{1s}(E)$ of $1s$ states via

$$|\mathcal{A}(E)|^2=\sqrt{\frac{m|E|}{2\pi^2\hbar^2}}\frac{D_{1s}(E)}{1-\exp\left(-2\sqrt{\frac{2m|E|}{\hbar^2}}R_E\right)}, \tag{15}$$

where R_E is the radius of the relevant empty sphere. Since, for a nondispersive band, the phase associated with each of the orbitals is unimportant, Eqs. (14) and (15) provide a simple way of estimating the density of electronic states in the asymptotic region corresponding to a typical tip-surface separation of the order of several ansgstroms. An STM image can then be simulated by plotting the logarithm of the normalized density of states in the vacuum region as a function of the coordinate of the tip in a plane parallel to the surface. Two STM images generated by using this procedure for positive and negative bias are shown in Fig. 5 together with a schematic drawing of the NiO (100) surface. These images show that at positive bias electrons tunnel mainly from the tip to the nickel sites while at negative bias they come out of the surface primarily from the oxygen sites. This explains the origin of the contrast reversal of STM images shown in Ref. 23.

Figure 6 shows two atomically resolved STM images taken at positive (a) and negative (b) sample biases. The relative positions of the images of the sublattices have been adjusted so that the bright Ni ions in (a) are coincident with the spaces between the bright O ions in (b) in accordance with the results of Ref. 23.

It is seen that there is much higher contrast at positive bias than at negative bias. This can also be explained on the basis of the model described above. Close inspection of the DOS shown in Fig. 3 reveals a small but distinguishable peak in the DOS for empty spheres situated above the *nickel* surface sites at the top of the valence band. A similar small peak can also be noticed in Fig. 4 at the bottom of the con-

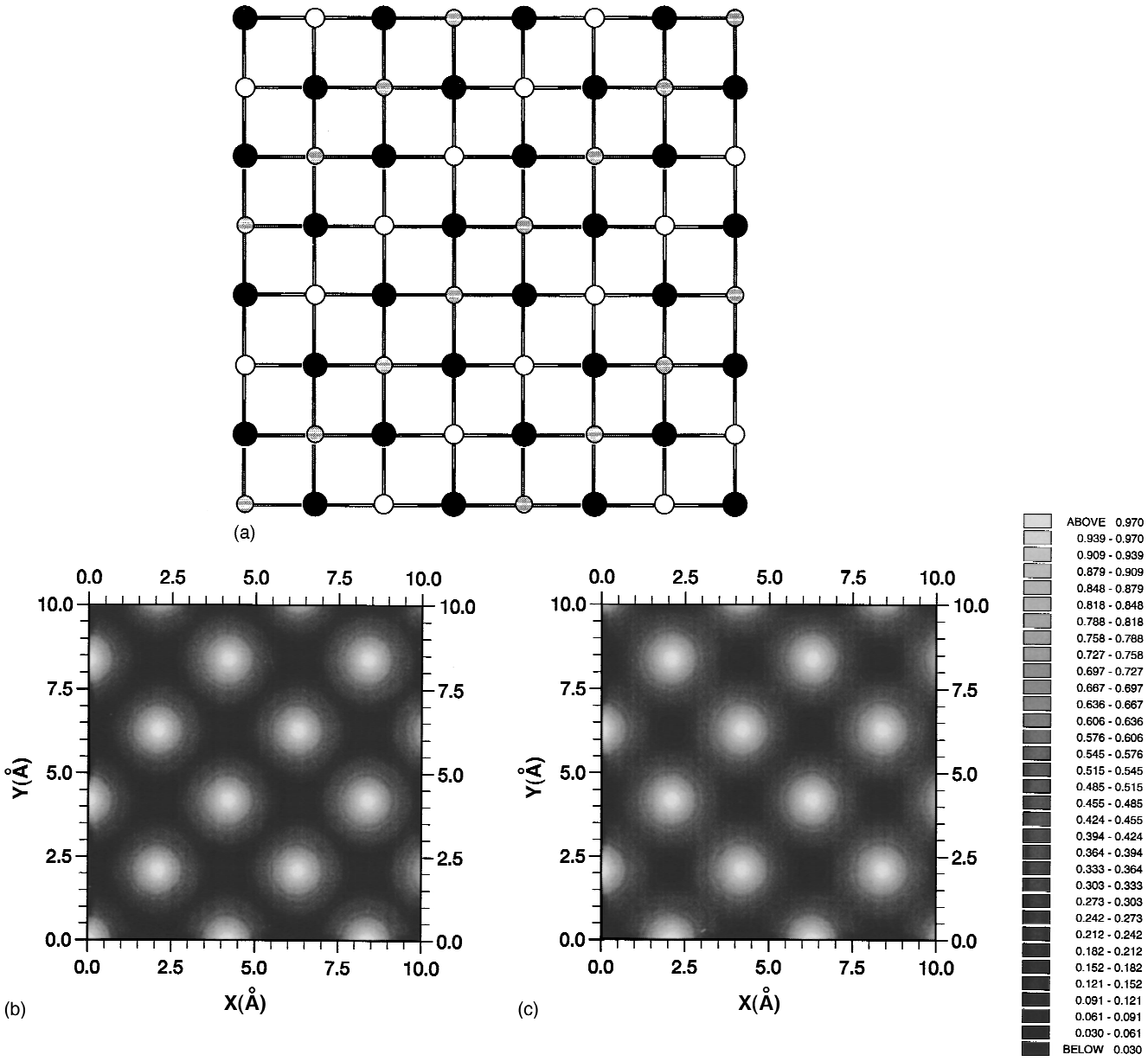

FIG. 5. (a) The (100) surface of nickel monoxide, top view. Oxygen sites are shown in black, nickel sites are shown in gray and white. In the antiferromagnetic ground state the white and gray sites belong to magnetic sublattices with opposite projection of momentum. (b) A simulated STM image of the (100) surface of NiO for $+2$ V sample bias assuming that a tip-surface separation equals ~ 4 Å. (c) A simulated STM image of the (100) surface of NiO simulated for -2 V sample bias for the tip-surface separation of ~ 4 Å. For cases (b) and (c) the absolute temperature was assumed to be 450 K. Note the contrast reversal in (b) and (c).

duction band for empty spheres situated above *oxygen* sites. Numerical integration of the DOS of the first layer of empty spheres over the energy interval between -0.4 eV and 0.1 eV (corresponding to the oxygen-derived $2p_z$-type surface state) shows that approximately 83% of its weight corresponds to the empty spheres above oxygen sites and 17% is associated with empty spheres above nickel sites. For the empty states peak at approximately $+3.4$ eV with respect to the top of the valence band (the nickel $3d_{3z^2-r^2}$-type surface state) the distribution of weights in the first vacuum layer is different, namely, 91% is now concentrated in the sphere above nickel sites while only 9% is in the spheres above oxygen sites.

The tunneling current is proportional to the density of states, D, times the barrier transmission coeffcient:

$$I \sim D \exp(-2d\sqrt{2m|E|/\hbar^2}). \tag{16}$$

Using this equation, we arrive at the following estimate for the corrugation height:

$$\delta d = d_{\mathrm{Ni}} - d_{\mathrm{O}} = \frac{1}{2}\sqrt{\frac{\hbar^2}{2m|E|}}\ln\left(\frac{D_{\mathrm{Ni}}}{D_{\mathrm{O}}}\right), \tag{17}$$

where the subscripts refer to the nickel and oxygen sites. From a slab calculation we know that the top of the valence band lies approximately 10 eV below the vacuum level. Substituting this value into Eq. (17) and using the ratios $D_{\mathrm{Ni}}/D_{\mathrm{O}} = 17/83$, 91/9 for filled and empty surface states, respectively, in the first layer of empty spheres, we obtain $\delta d \sim 0.49$ Å for a negative and $\delta d \sim 0.88$ Å for a positive

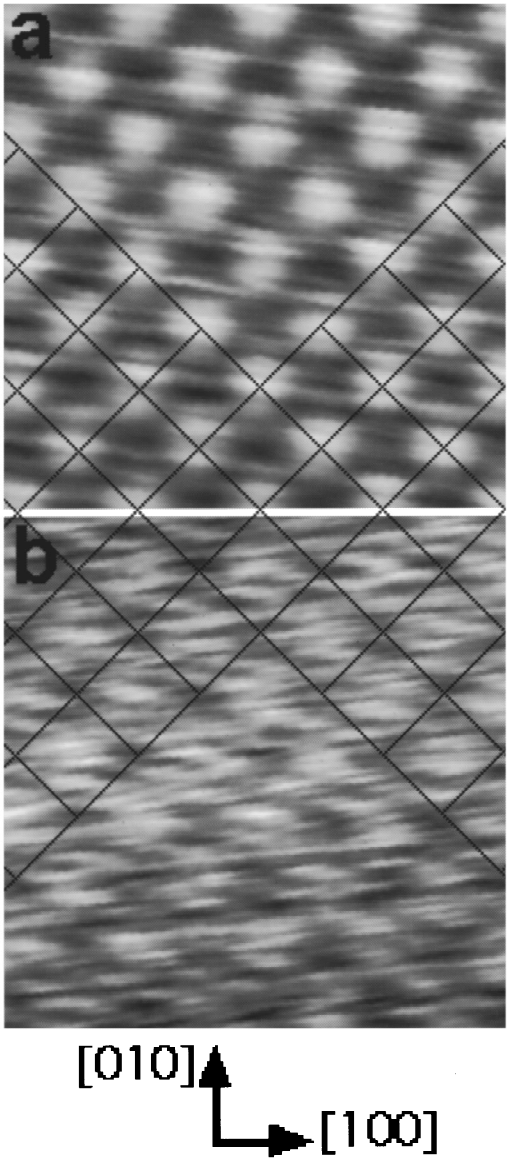

FIG. 6. Empty states (a), (+1.1 V sample bias, 1.0 nA tunneling current) and filled states (b), (−1.5 V sample bias, 1.0 nA tunneling current) atomically resolved STM images of the (100) surface of NiO. The two images have been presented so that the bright Ni sites seen in (a) are located between the bright O sites imaged in (b) (see text). The average corrugation heights are approximately 0.3 Å in (a) and 0.15 Å in (b).

applied bias. Therefore we predict the contrast to be two times higher at a positive bias than at a negative bias. This agrees qualitatively with the experimental images shown in Fig. 6. Our calculated corrugation heights are both larger than those observed experimentally, which suggests that in the experiment the tip was scanned at a height above the first layer of empty spheres, i.e., higher than 2.1 Å.

There is another factor which affects the STM images. The filled oxygen surface states are situated at a much lower energy than the empty nickel surface states. As a result of this energy difference, the rate of exponential decay of the oxygen surface states into the vacuum is greater than the rate characterizing the decay of the nickel surface states. Therefore, the tunneling current which can be achieved at a given tip-surface separation, turns out to be much lower in the case of tunneling via oxygen sites (negative bias) than in the case of tunneling via nickel sites (positive bias). Therefore, to obtain the same level of tunneling current at a negative bias as at a given positive bias, the tip has to be closer to the surface. This may result in a considerable increase in tip-surface interaction and a higher noise level, which we suspect may be the principal reason for the difference in noise levels seen in Figs. 6(a) and (b).

V. CONCLUSIONS

We have reported the results of an application of the LSDA+U method to the electronic structure of the (100) surface of nickel monoxide. We found that the electronic structure of the (100) surface is of the charge transfer type and is characterized by the presence of strong on-site repulsion between valence electrons in d orbitals of nickel ions. We found two types of surface state associated with the (100) termination of the lattice, one (filled) state originating primarily from p_z orbitals of oxygen ions and another (empty) originating primarily from $d_{3z^2-r^2}$ orbitals of nickel ions. These surface states explain the origin of the contrast reversal of STM images observed experimentally when the sample bias is reversed.

ACKNOWLEDGMENTS

We are grateful to Dave Goddard, David Pettifor, and Marshall Stoneham for stimulating discussions. We would like to thank Paul Wincott, Christiane Muggelberg, and Geoff Thornton for involvement with the experimental work. Computations were performed in the Materials Modelling Laboratory of the Department of Materials. Financial support from British Nuclear Fuels plc (BNFL) is gratefully acknowledged. We also acknowledge financial support from EPSRC Grant No. GR/K08161. A.I.L. thanks the Ψ_K network for the provision of a travel grant.

[1] V. E. Henrich and P. A. Cox, *The Surface Science of Metal Oxides* (Cambridge University Press, Cambridge, England 1994).

[2] S. G. Davison and M. Stęślicka, *Basic Theory of Surface States* (Clarendon Press, Oxford, 1992).

[3] C. Noguera, *Physics and Chemistry at Oxide Surfaces* (Cambridge University Press, Cambridge, England, 1996).

[4] D. Adler, in *Solid State Physics: Advances in Research and Applications*, edited by F. Seitz, D. Turnbull, and H. Ehrenreich (Academic Press, New York, 1968), Vol. 21.

[5] O. K. Andersen, H. L. Skriver, H. Nohl, and B. Johansson, Pure Appl. Chem. **52**, 93 (1980).

[6] K. Terakura, A. R. Williams, T. Ogichi, and J. Kübler, Phys. Rev. Lett. **52**, 1830 (1984); Phys. Rev. B **30**, 4734 (1984).

[7] J. Kübler and A. R. Williams, J. Magn. Magn. Mater. **54-57**, 603 (1986).

[8] G. A. Sawatzky and J. W. Allen, Phys. Rev. Lett. **53**, 2339 (1984).

[9] S. Hüfner, Adv. Phys. **43**, 183 (1994).

[10] Z.-X. Shen and D. S. Dessau, Phys. Rep. **253**, 1 (1995).
[11] F. Aryasetiawan and O. Gunnarsson, Phys. Rev. Lett. **74**, 3221 (1995).
[12] F. Manghi, C. Calandra, and S. Ossicini, Phys. Rev. Lett. **73**, 3129 (1994); C. Calandra and F. Manghi, Phys. Rev. B **50**, 2061 (1994).
[13] M. D. Towler, N. L. Allan, N. M. Harrison, V. R. Saunders, W. C. Mackrodt, and E. Apra, Phys. Rev. B **50**, 5041 (1994).
[14] V. I. Anisimov, J. Zaanen, and O. K. Andersen, Phys. Rev. B **44**, 943 (1991).
[15] A. I. Liechtenstein, V. I. Anisimov, and J. Zaanen, Phys. Rev. B **52**, R5467 (1995).
[16] J. Zaanen and G. A. Sawatzky, Can. J. Phys. **65**, 1262 (1987); Prog. Theor. Phys. Suppl. **101**, 231 (1990).
[17] V. I. Anisimov, I. V. Solovyev, M. A. Korotin, M. T. Czyzyk, and G. A. Sawatzky, Phys. Rev. B **48**, 16 929 (1993).
[18] K. Akimoto, Y. Sakisaka, M. Nishijima, and M. Onchi, J. Phys. C **11**, 2535 (1978).
[19] A. Freitag, V. Staemmler, D. Cappus, C. A. Ventrice, K. Al Shamery, H. Kuhlenbeck, and H.-J. Freund, Chem. Phys. Lett. **210**, 10 (1993).
[20] A. Gorschlüter and H. Merz, Phys. Rev. B **49**, 17 293 (1994).
[21] M. R. Castell, C. Muggelberg, G. A. D. Briggs, and D. Goddard, J. Vac. Sci. Technol. B **14**, 966 (1996).
[22] C. Muggelberg, M. R. Castell, G. A. D. Briggs, and D. Goddard, Surf. Rev. Lett. (to be published).
[23] M. R. Castell, P. L. Wincott, N. G. Condon, C. Muggelberg, G. Thornton, S. L. Dudarev, A. P. Sutton, and G. A. D. Briggs, Phys. Rev. B **55**, 7859 (1997).
[24] V.-C. Lee and H.-S. Wong, J. Phys. Soc. Jpn. **50**, 2351 (1981).
[25] L. F. Mattheiss, Phys. Rev. B **5**, 290 (1972).
[26] M. A. van Veenendaal and G. A. Sawatzky, Phys. Rev. Lett. **70**, 2459 (1993).
[27] D. Alders, F. C. Voogt, T. Hibma, and G. A. Sawatzky, Phys. Rev. B **54**, 7716 (1996).
[28] S. L. Dudarev, D. Nguyen Manh, and A. P. Sutton, Philos. Mag. B **75**, 613 (1997).
[29] E. Fradkin, *Field Theories of Condensed Matter Systems* (Addison-Wesley, Reading, Massachusetts, 1991).
[30] R. P. Feynman, *Statistical Mechanics* (Benjamin, Reading, Massachusetts, 1972).
[31] V. I. Anisimov and O. Gunnarsson, Phys. Rev. B **43**, 7570 (1991); for *d* electrons the two parameters U and J can be expressed in terms of the Slater integrals F^0, F^2, and F^4 as $U=F^0$ and $J=(F^2+F^4)/14$, see, for example, I. V. Solovyev, P. H. Dederichs, and V. I. Anisimov, *ibid.* **50**, 16 861 (1994).
[32] S. Yu. Savrasov and D. Yu. Savrasov, Phys. Rev. B **46**, 12 181 (1992).
[33] F. P. Netzer and M. Prutton, J. Phys. C **8**, 2401 (1975); M. R. Welton-Cook and M. Prutton, *ibid.***13**, 3993 (1980).
[34] C. G. Kinniburgh and J. A. Walker, Surf. Sci. **63**, 274 (1977).
[35] J. J. M. Pothuizen and G. A. Sawatzky, in *Abstracts of the 1995 Materials Research Society Fall Meeting* (Materials Research Society, Boston, MA, 1995), p. 267.
[36] S. Sugano, Y. Tanabe, and H. Kamimura, *Multiplets of Transition-Metal Ions in Crystals* (Academic Press, New York, 1970).
[37] M. F. Crommie, C. P. Lutz, D. M. Eigler, and E. J. Heller, Surf. Rev. Lett. **2**, 127 (1995).
[38] U. Diebold, J. F. Anderson, K.-O. Ng, and D. Vanderbilt, Phys. Rev. Lett. **77**, 1322 (1996).